

# Atomically Resolved Spin-Dependent Tunnelling on the Oxygen-Terminated Fe<sub>3</sub>O<sub>4</sub> (111)

N. Berdunov, S. Murphy, G. Mariotto, and I. V. Shvets

SFI Nanoscience Laboratory, Trinity College, Dublin 2, Ireland

Spin polarization of the magnetite surface/interface and the impact of surface defects on it are of our interest. Under oxidation preparation conditions magnetite (111) surface reconstructs to a highly ordered superlattice. This surface reconstruction represents an oxygen-termination of the magnetite bulk. We employ spin-polarized (SP) STM to study a spin-dependent tunnelling between a magnetite (111) sample and an antiferromagnetic tip through a vacuum barrier at room temperature. Atomic scale STM images show significant magnetic contrast corresponding to the variations in the local surface states induced by oxygen vacancies. The local variations of the tunnelling magnetoresistance around these point defects correspond to 250%. By employing SP-STM measurements and *First principles* calculations we could conclude that a top-surface oxygen layer considerably changes the SP properties of the magnetite interface.

## PACs

75.25.+z, 75.30.Pd, 75.70.Cn

**Keywords:** Spin-polarized STM; Magnetic interfaces; Nanostructured surfaces, tunnelling magnetoresistance.

## Introduction

Magnetite, Fe<sub>3</sub>O<sub>4</sub>, predicted to be a half-metallic ferromagnet, attracts a lot of interest from the spin electronics community. It is expected that a magnetic tunnel junction (MTJ) with a Fe<sub>3</sub>O<sub>4</sub> electrode could exhibit a high Tunnelling Magnetoresistance (TMR) effect.

In practice, at room temperature such MTJs do not demonstrate a sizable magnetoresistance and at low temperature the MR values reported are still much lower than expected<sup>1 2</sup>. However, the photoelectron spectroscopy measurements on the magnetite surface do show much greater values of the Spin Polarization (SP)<sup>3</sup>. It was suggested that this reduction of SP is due to the disorder at the electrode/barrier drastically changing the spin-polarized properties of the interface<sup>4 5 6 7</sup>. In complex structures, like magnetite, surface can represent a number of non-identical terminations, which possess a variety of spin-electronic properties. For example, it was shown that an oxygen layer deposited on a magnetic electrode could change MTJ properties drastically, even reversing the sign of spin-polarization<sup>8</sup>. Therefore, an understanding of the relationship between spin-electronic properties and the structure of the surfaces/interfaces at the nanometer and atomic scale is of much interest.

In the present work we apply Spin Polarized Scanning Tunnelling Microscopy (SP-STM) measurements to analyze the electronic structure of the oxygen-terminated magnetite (111) surface. We aim to understand the impact of the point defects on the surface electronic structure and on the spin dependent tunnelling between a magnetite sample and an antiferromagnetic MnNi tip through a vacuum barrier. The potential of SP-STM as a useful tool to study the surface magnetic properties has been demonstrated in recent experimental and theoretical works<sup>5 9 10</sup>. Spin-dependent tunnelling can be achieved by selecting the tunnelling conditions for the majority and minority spin states. Such kind of the selective SP-STM techniques can be broadly divided into two groups. The first one utilizes a ferromagnetic tip with the magnetization switched by a local magnetic field<sup>11 12</sup>.

However, there are no reports of atomic resolution achieved with this approach so far. The second one uses an antiferromagnetic tip to scan the surface when the magnetic field applied is strong enough to alter a sample magnetization. In earlier theoretical work<sup>13</sup> it has been shown that spin-contrast can be achieved in the case of tunnelling between an antiferromagnet and ferromagnet electrodes. The first STM experiments using antiferromagnetic tips have been reported in [<sup>14</sup>]. More recently, atomically resolved SP-STM data employing Cr<sup>15</sup> and MnNi<sup>16</sup> tips have been reported. It is worth to point out that SP-STM does not provide the absolute value of the local magnetic moment, as there are uncertainties in the tunnelling gap distance and the surface/tip states contribution to tunnelling. Nonetheless, by analyzing SP-STM results, in particular, with the help of *first principles calculations*, further insights into the local density of states on the surface and their contribution to the tunnel current can be obtained<sup>9</sup>.

## Experimental

The experiments have been performed in ultra-high vacuum (UHV) at room temperature, using scanning tunnelling microscopy (STM), low-energy electron diffraction (LEED) and Auger electron spectroscopy (AES). In our SP-STM measurements, MnNi tips made of antiferromagnetic alloy were employed. The tip preparation is discussed in detail in [<sup>17</sup>].

A magnetite (111) synthetic single crystal has been used in these experiments. The crystal structure of magnetite allows for six ideal bulk terminations in the (111) plane (Fig.1). In the present Letter we limit our discussion by considering the case of oxygen terminations.

Two of them represent close-packed oxygen layers with identical atomic periodicities.

One appears as an oxygen monolayer on top of an octahedral Fe layer, while the other covers a multilayer of tetrahedral and octahedral Fe atoms.

As the different terminations correspond to the different subsurface stoichiometry, choosing either a reduction or an oxidation sample preparation procedure, we were able to achieve two stable terminations. One is referred in [18] as Fe-tetrahedral termination, another represents an oxygen termination with a long-range order on the surface<sup>19</sup>. The latter is a subject of this study.

### ***Oxygen-induced surface reconstruction***

The magnetite sample was annealed in UHV at  $950\pm20$  K followed by a short anneal in an oxygen atmosphere of  $10^{-6}$  mbar at 950K for 15 min, which was in turn followed by cooling in the oxygen atmosphere. This sample preparation procedure leads to the formation of a well-defined hexagonal superlattice with a periodicity of  $42\pm3$  Å. This superstructure is highly regular and covers almost the entire sample surface. The high-resolution STM image in Fig.2(a) shows the atomic arrangement within the superstructure. One can see that the superstructure consists of three distinct areas, marked as areas I, II and III. Detailed analysis shows that area I has a periodicity of  $3.1\pm0.1$  Å, while areas II and III have a periodicity of  $2.8 \pm 0.1$  Å along the [011] direction, which is consistent with the LEED pattern<sup>19</sup>. As we have shown in an earlier publication<sup>19</sup>, the superstructure depicts an oxygen-terminated magnetite bulk, which reconstructs due to

the electron-lattice instability, a polaron- or a charge density wave-like. Thus, the STM image in Fig.2(a) represents a lattice of oxygen sites on the top of iron layer. A number of defects seen in Fig.2(a) represent the missing oxygen atoms (oxygen vacancies). We have further shown<sup>20</sup> that at a critical density of oxygen vacancies of some 30%, the superstructure disappears. This means that the oxygen topmost layer is responsible for the electronic transformation in the sub-surface layer, and for the Fe-states changes leading to the superstructure formation.

In our SP-STM experiments a magnetic field of 60 mT was applied parallel to the surface during the STM scan. We have verified *ex-situ* by vibrating sample magnetometer that this magnetic field is strong enough to fully magnetize the sample. Unfortunately, the large magnetostriction effect in the magnetic materials like magnetite does not allow one to switch the magnetic field during the scan. The STM images were taken on the same sample within the space of a few hours between the non-magnetic and magnetic experiments, no additional sample treatment between the experiments were performed. The sample was subsequently scanned without magnetic field to ensure that there was no significant contaminant adsorption during the experiment. The notion of the contaminants was also checked by switching bias polarity.

The spin-contrast achieved in STM images when the magnetic field switched off/on is demonstrated in Fig2(a,b) respectively. As it can be seen, the appearance of the superstructure and corrugation between different areas is almost unaffected by the magnetic field. However, the major changes occur in proximity of the oxygen vacancies.

Three bright spots appear in the vicinity of the defects as can be seen in Fig.2(b). The 6 Å separation between the spots and their positions correspond to those of Fe ions in the layer underneath the topmost oxygen lattice. The effect becomes more pronounced when the density of defects rises (Fig.2c).

We can quantify the observed spin polarized effect in terms of the tunnelling conductance variation around the surface defects

$$\sigma = (G_{60mT} - G_0)/G_0, \quad (1)$$

where  $G_{60mT}$ ,  $G_0$  are the tunnelling conductances with and without the applied magnetic field. To estimate the tunneling conductances, we can use a simplified approach where the tunnel current is proportional to the bias voltage  $U$ , the distance ( $1/d$ ), the energy of the barrier between the two electrodes  $\varphi$  and constant  $A = 1.025$

$$I_t \sim (U/d_i) \exp(-A \varphi_i^{-1/2} d_i)$$

Where index  $i=1,2$  corresponds to the case when the tip is positioned above an oxygen vacancy and an oxygen atom, respectively (see Fig.3). In our experiment, the tunnel current is  $I_t=0.1$ nA, the bias voltage  $U=1$ V. The tip displacement over the point of the corrugation maxima in the STM image is equal to 0.3 Å. Assuming that the tip-surface distance is 5 Å, we can calculate the change in the barrier energy and the corresponding tunnelling conductance of the 5 Å tunnelling gap. Their substitution into formula (1) gives us a  $\sigma$  value of 2.5. This value indicates a significant spin polarization effect in the

presence of the defects (oxygen vacancies) on the surface. Our assumption regarding the tip-sample distance is based on the conclusion of the paper [21, 22] and our coarse estimation following the method proposed in [22]. In fact, even the broad distance range 4-10 Å will still give us high value of  $\sigma$  from 3.8 to 0.9.

The formula (1) we used is similar to the *Julliere*'s definition of the TMR [23]:

$TMR = (G_p - G_{ap})/G_{ap} * 100\%$ . Where  $G_p$ ,  $G_{ap}$  are the tunnelling conductances in case of parallel and antiparallel magnetisation at the electrodes. Assuming  $G_{60mT} = G_p$ ;  $G_0 = G_{ap}$ , that corresponds to a 250% TMR effect observed. Although, in the absence of a magnetic field it is not necessarily true that we fulfill the conditions for the minimum conductance, so that the correct correspondence is  $G_0 \geq G_{ap}$ . Therefore the calculated TMR value should be taken as the lower limit.

### *First Principles Calculations and Discussion*

To analyze the SP-properties of the oxygen-terminated magnetite (111) surface we have performed DFT calculations for the ideal oxygen-terminated magnetite (111) vacuum slab (vacuum/magnetite/vacuum interface) and also in the presence of a surface defect. The CASTEP program [24] as a module of Materials Studio was used in our calculations. A one unit cell vacuum slab similar to that shown in Fig.1 has been constructed. The local spin-density LSDA functional based on ultrasoft pseudopotentials was used to optimize the surface geometry, first, and then calculate the local density of states. A plane

wave cutoff of 260eV and a (3x3x1) grid of  $k$ -points were chosen. We limit our discussion presenting the calculation for an oxygen-termination on top of an Fe-octahedral layer (Fig.1(b)).

It is known that in transition metals the 3d electrons make a large contribution to the tunnelling current. In the case of the oxygen-terminated surface, one may not expect a tunnelling contribution from the oxygen p-states. However, on the surface the hybridization between oxygen p-states and transition metal d-states changes the situation altering the oxygen p-orbitals from insulating to conductive<sup>7</sup>. The results of our calculations support this viewpoint: the oxygen states on the magnetite surface contribute to the tunnelling. The layer-projected partial density of states in Fig.4 shows significant p-d states hybridization between the topmost oxygen anions and the Fe ions in the layer underneath. The p-states of the oxygen anions are shifted towards the Fermi level eliminating the band gap (Fig.4a). This effect almost disappears in the second oxygen layer (Fig.4c), where the oxygen p-states are similar to those in the bulk. These predictions are in good agreement with our experimental data. We readily resolve 3Å periodicity of the oxygen sites at bias voltages ranging from -1V to -0.5V, while this lattice disappears if we tunnel in/from the surface states about and above Fermi level (bias from -0.3 to +1V). The absence of the Fe-lattice in STM images taken at positive bias (tunnelling to the unoccupied Fe-states) can be explained by scattering of the tunnelling electrons in closed-packed oxygen layer.

As mentioned earlier, the periodicity and position of the maxima appearing around an oxygen vacancy (Fig.2(b)) correspond to the iron sites in the layer below the topmost oxygen layer. As the image Fig.2(b) was taken with the bias voltage -1V, we should expect a significant spin-polarization at 1eV below the Fermi-level. Induced by the p-d hybridization the spin-polarization of the surface oxygen is much smaller than spin-polarization of the Fe-states (Fig.4(a,b)). There is a corresponding peak in the majority of the Fe-octahedral d-states 2eV below Fermi level.

The next calculations were performed for 2x2 supercell (which is still smaller than the actual reconstruction (7x7) unit cell) with and without a defect present. Fig.4b shows the uniform distribution with the maxima of spin-up states above each oxygen atom in the case of a non-defected surface. In contrary, the presence of the oxygen vacancy alters the spin polarization of the surface oxygen affecting the neighbor atoms (Fig.4c). The integrated spin density has an almost uniform distribution in both cases.

As the calculations have been done for a relaxed oxygen termination which does not reconstruct into superlattice, the comparison with the experiment is rather qualitative. Nevertheless, the main conclusion can be drawn that the closed-packed oxygen layer plays crucial role, changing the spin-polarized properties of the magnetite interface. Either surface states scattering or the exchange interaction between Fe ions mediated by surface oxygen [25] alters the spin-polarization at the interface. That prevents the contribution of the 3d-states to tunneling in the case of non-defected oxygen termination.

## Conclusions

Investigating the tunnelling between an oxygen-terminated  $\text{Fe}_3\text{O}_4$  (111) surface and an antiferromagnetic tip across a vacuum barrier, we observed the significant changes in TMR values, which are localized in the vicinity of oxygen vacancies on the surface. Employing first-principles calculations, we conclude that a surface oxygen layer plays a decisive role in the spin-polarized properties of the magnetite interface, which consists of the reduction of spin-polarization in case of the closed oxygen layer on the surface.

#### ACKNOWLEDGMENTS

This work was supported by Science Foundation of Ireland (SFI) under contract 00/PI.1/C042.

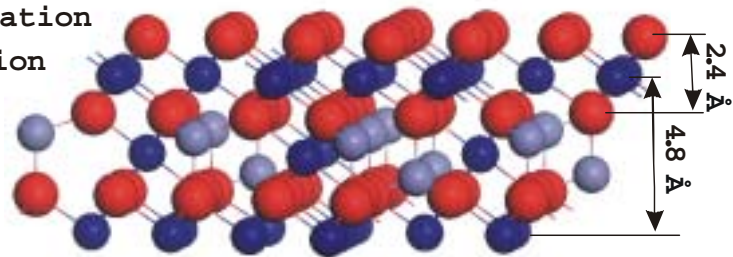
a

$\text{Fe}_3\text{O}_4$  [111] slab

oxygen termination

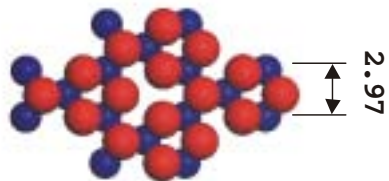
$\text{Fe}_{\text{oct}}$  termination

Fe-multilayer  
termination



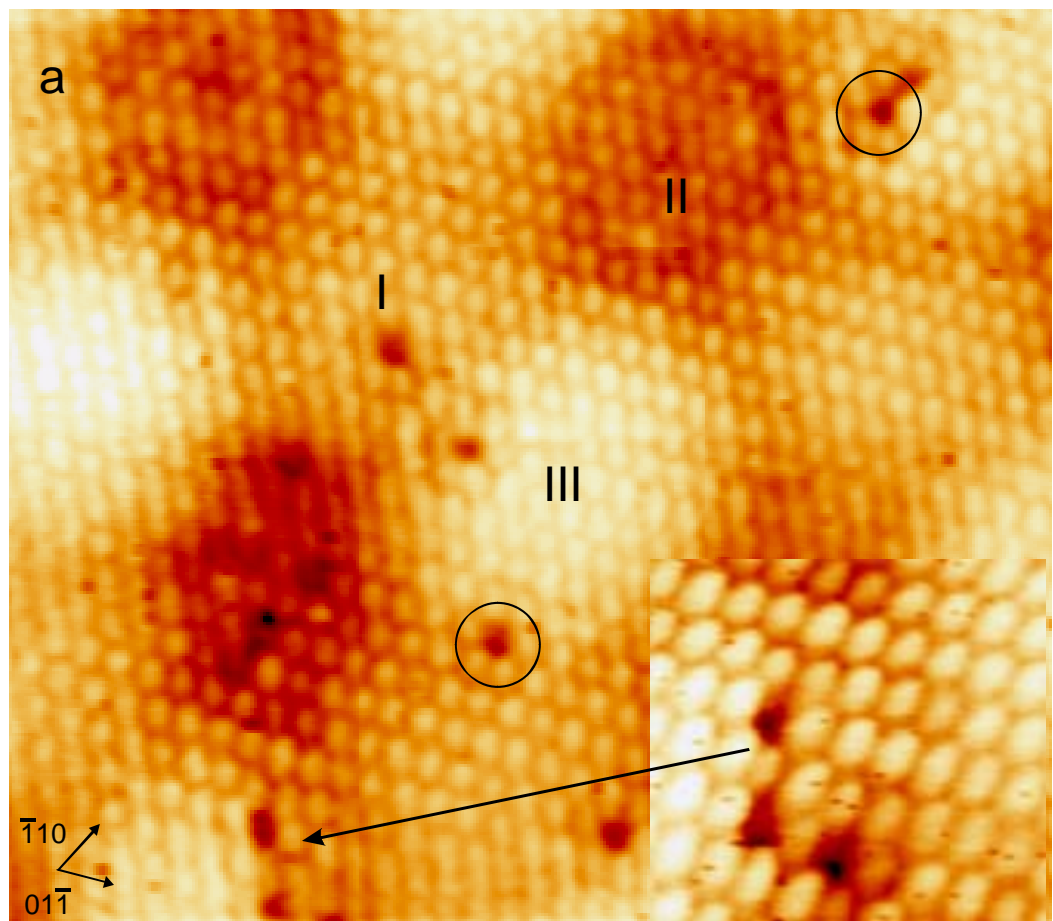
b

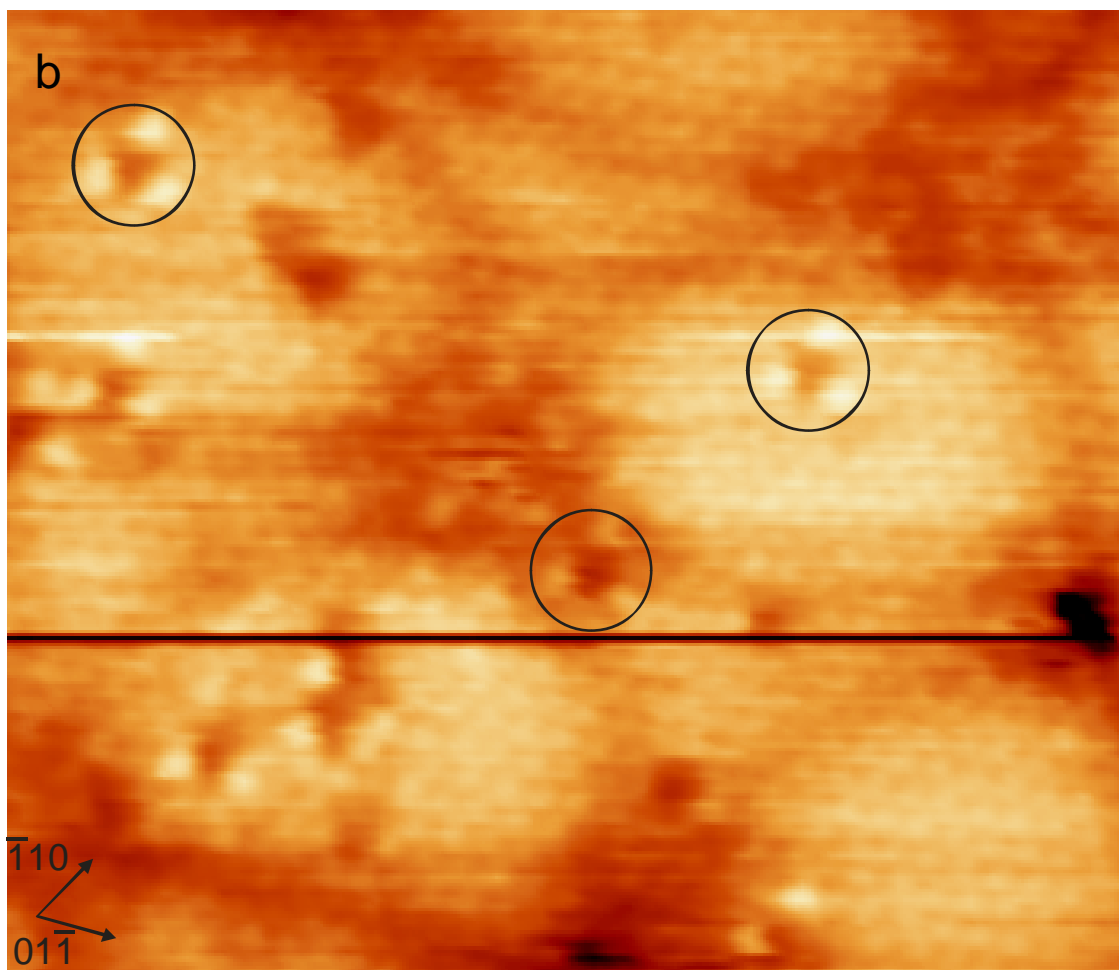
Oxygen termination



● -  $\text{O}^{2-}$   
● -  $\text{Fe}_{\text{oct}}^{2+, 3+}$  (B-site)  
● -  $\text{Fe}_{\text{tet}}^{3+}$  (A-site)

**Fig.1. Magnetite [111] vacuum slab (a) and oxygen termination on the top of Fe-octahedral layer (b).**





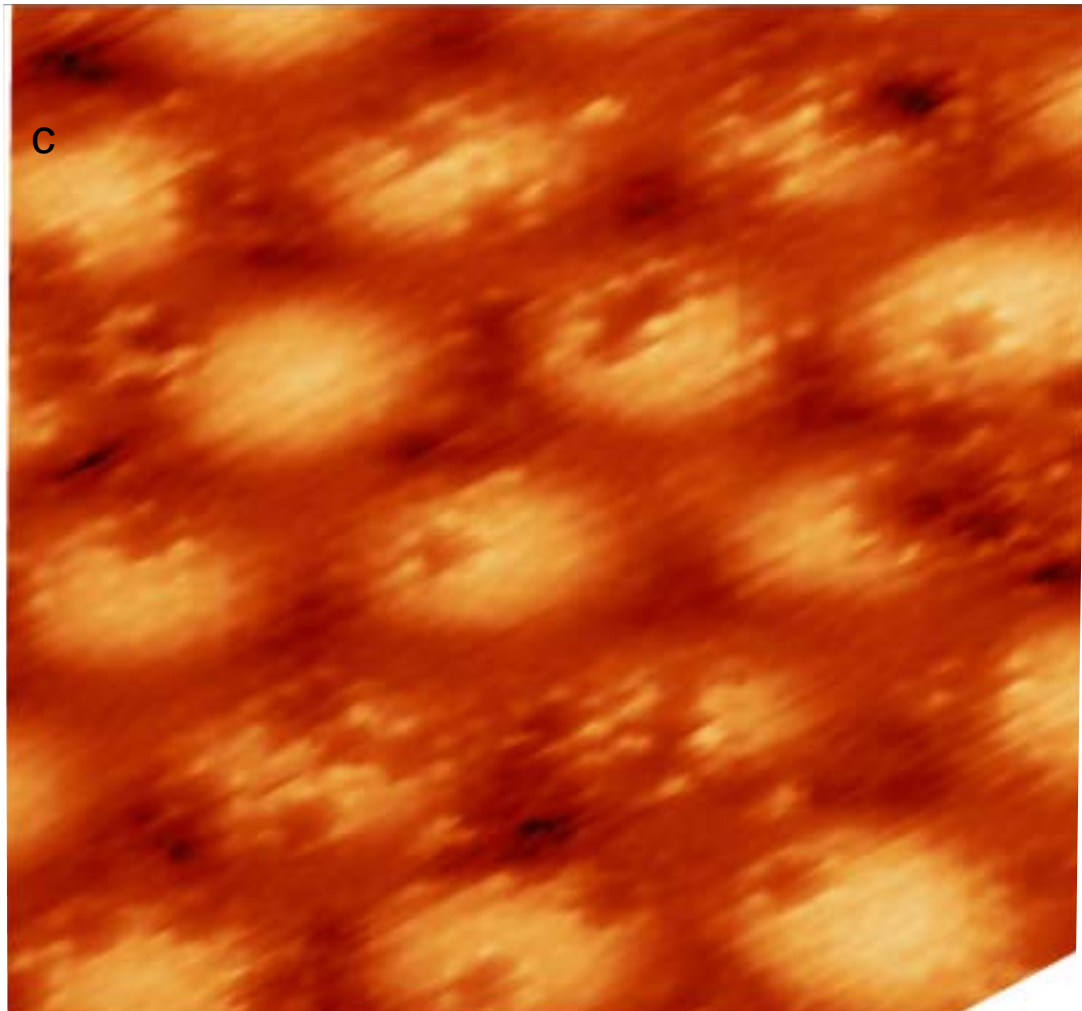


**Fig.2. STM images (10.5×8.5 nm<sup>2</sup> , 9×8 nm<sup>2</sup> and 12.0×17.5 nm<sup>2</sup>) of the superstructure without (a) and with magnetic field (b,c) . Blue circles mark the missing oxygen defects in the topmost surface layer. (b) In a case of the applied magnetic field, three bright spots appeared around defect correspond to the Fe sites with 6 Å interatomic distance; (c) a case of higher density defects on the surface. (V<sub>bias</sub>= -1.0 V, I<sub>t</sub> = 0.1 nA, MnNi tip in both cases). Insert in the figure 2a represent a high-resolution image of the proximity of defects.**

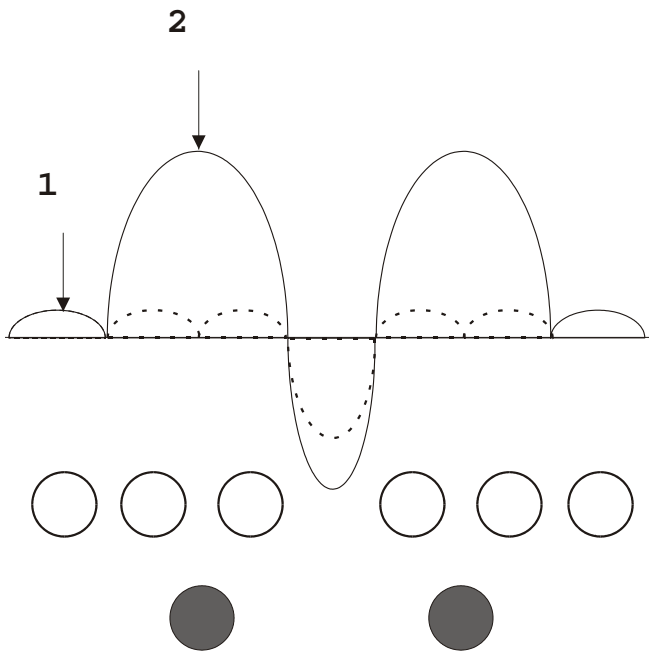


**Fig.3. (a) Schematic representative of the STM line profile (solid curve – magnetic field applied; dashed line – no magnetic field) above an oxygen-defect. (Oxygen atoms are white balls, Fe atoms – grey; tip position 2 indicate the magnetic contrast maxima seen in Fig.2(b)).**

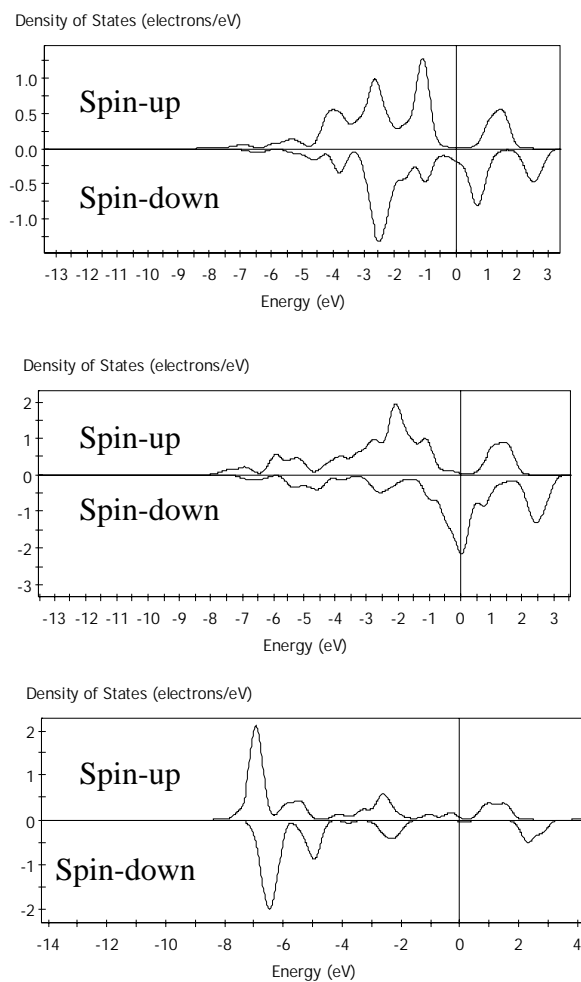


**Fig. 4. (a) Partial density of states**  
**corresponding: (top) 2p (O) states in**  
**closed-packed oxygen topmost layer;**  
**(middle) 3d (Fe) in the Fe-octahedral**  
**layer, next to the topmost oxygen**  
**layer; (bottom) 2p (O) states in the**  
**third layer.**

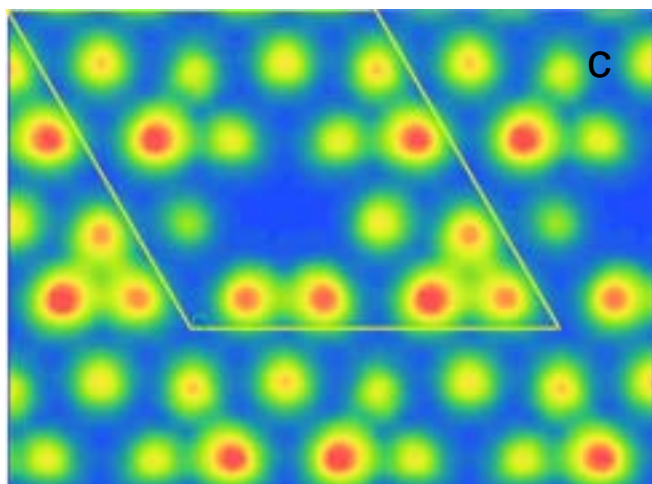
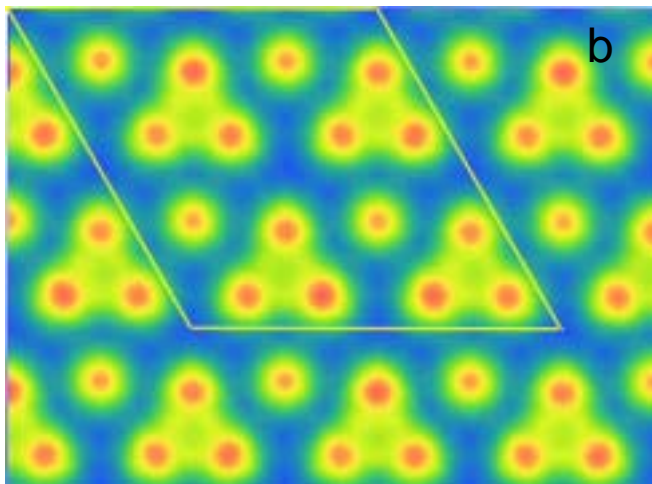


**Fig. 4. (b,c)** Spin-up electron density above the oxygen terminated surface: ideal surface layer (b); and with the presence of oxygen vacancy (c). The sketch of energy range [ $E_F - 1\text{eV}, E_F$ ] was chosen to make it reliable with STM data ( $V_{\text{bias}} = -1\text{V}$ ). The (2x2) supercell used in the calculations is marked.

---

- [1] G. Hu and Y. Suzuki, *Phys. Rev. Lett.* **89**, 276601 (2002).
- [2] P. Seneor, A. Fert, J.-L. Maurice, F. Montaigne, F. Petroff, and A. Vaurès, *Appl. Phys. Lett.* **74**, 4017 (1999).
- [3] Yu. S. Dedkov, U. Rüdiger, and G. Güntherodt, *Phys. Rev. B* **65**, 064417 (2002).
- [4] J. S. Moodera, J. Nowak, and J. M. van de Veerdonk, *Phys. Rev. Lett.* **80**, 2941 (1998).
- [5] H. F. Ding, W. Wulfhekel, J. Henk, P. Bruno, and J. Kirschner, *Phys. Rev. Lett.* **90**, 116603 (2003).
- [6] S. Zhang, P. M. Levy, A. C. Marley, and S. S.P. Parkin, *Phys. Rev. Lett.* **79**, 3744 (1997).
- [7] E. Y. Tsymbal, O. N. Mryasov, and P. R. LeClair, *J. Phys.: Condens. Matter* **15**, R109 (2003).
- [8] I. I. Oleynik and E. Y. Tsymbal, *J. Appl. Phys.* **93**, 6429 Part 2 (2003).
- [9] W. A. Hofer and A. J. Fisher, *Surf. Sci. Lett.* **515**, L487 (2002).
- [10] D. Wortmann, S. Heinze, P. Kurz, G. Bihlmayer, and S. Blugel, *Phys. Rev. Lett.* **86**, 4132 (2001).
- [11] M. Bode, *Rep. Prog. Phys.* **66**, 523 (2003).
- [12] U. Schlickum, *Appl. Phys. Lett.* **83**, 2016 (2003).
- [13] A. Minakov and I. V. Shvets, *Surf. Sci.* **236**, L377 (1990).

---

- [14] I. V. Shvets, R. Wiesendanger, D. Burgler, G. Tarrach, H. J. Guntherodt, and J.M. D. Coey, *J. Appl. Phys.* **71**, 5489 (1992).
- [15] A. Kubetzka, M. Bode, O. Pietzsch, and R. Wiesendanger, *Phys. Rev. Lett.* **88**, 57201 (2002).
- [16] G. Mariotto, S. Murphy, and I. V. Shvets, *Phys. Rev. B* **66**, 245426 (2002).
- [17] S. F. Ceballos, G. Mariotto, S. Murphy, and I. V. Shvets, *Surf. Sci.* **523**, 131 (2003).
- [18] Sh. K. Shaikhutdinov, M. Ritter, X.-G. Wang, H. Over, and W. Weiss, *Phys. Rev. B* **60**, 11062 (1999).
- [19] I. V. Shvets, N. Berdunov, G. Mariotto, and S. Murphy, *Europhys. Lett.* **63**, 867 (2003).
- [20] N. Berdunov, S. Murphy, G. Mariotto, and I. V. Shvets, *Phys. Rev. B* **submitted**, (2003); also [arXiv:cond-mat/0403238](https://arxiv.org/abs/cond-mat/0403238)
- [21] W.A. Hofer, A.J. Fisher, R.A. Wolkow, P. Grutter, *Pys.Rev.Lett.* **87**, 236104, 2001
- [22] W.A. Hofer, *Prog. Surf. Sci.* **71**, 147, 2003
- [23] M. Julliere, *Phys. Lett. A* **54**, 225 (1975).
- [24] Segall M. D., Lindan P. J. D., Probert M. J., Pickard C. J., Hasnip P. J., Clark S. J. and Payne M. C., *J. Phys. Condens. Matter*, **14** (2002) 2717.
- [25] D. D. Bagrets , A. Bagrets , A. Vedyayev , and B. Dieny , *Phys. Rev. B* **65**, 064430 (2002).